

TUNGSTEN OXIDE NANOSTRUCTURES SYNTHESIS BY SPIN COATING TECHNIQUE: STUDY THE ANNEALING EFFECT ON PHYSICAL PROPERTIES

N. R. ALABDALI, A. RAMIZY*

Physics Department, College of Sciences, University of Anbar, Anbar, Iraq

Tungsten oxide (WO_3) thin films were deposited on Si substrates using a spin-coating technique with 300 rpm for 60 Sec at room temperatures. The thin film deposit properties were investigated before and after annealing at temperatures of (400) °C for 1/2 hr. The structural, morphology, and optical properties of the thin films were characterized by using X-ray diffraction (XRD), Atomic force microscopy (AFM) and Photoluminescence spectra (PL). X-ray diffraction patterns showed that the films with hexagonal structure within the nano scale which confirmed by an increase in the broadening of XRD spectra. and reduction in crystallite size, on the other hand the results showed that the annealing temperature was enhanced the thin films structural properties. Atomic force microscope showed a sponge-like structure is produced. FE-SEM images showed a homogeneously dispersed and covering the substrate surface with range about 10-30nm. EDX analysis also indicates that no other element or impurity found in the fabricated sample. Photoluminescence spectra showed blue shift luminescence and the band gap energy increased from 3.45 to 3.48 eV as layer thickness increased.

(Received July 27, 2019; Accepted December 2, 2019)

Keywords: Tungsten oxide, Spin coating, Annealing effect, Nanostructures

1. Introduction

Tungsten oxide (WO_3) is a wide band gap n-type metal oxide semiconductor with outstanding electrochromic and gas sensing properties [1,2]. WO_3 possess distinctive physical and chemical properties that make it suitable for technological applications as transparent electrochromic devices, selective catalysts for oxidation and reduction reactions or transparent conducting electrodes [3–6]. WO_3 has been proving to be highly sensitive even to very low concentrations of toxic gases such as NO_x , H_2S , NH_3 and CO [7–10]. Gas sensing properties of WO_3 make it suitable for various applications such as environmental monitoring, automotive exhaust monitoring and currently in medical diagnostics for the detection of toxic gases exhausted by patients suffering from various heart and lung diseases [11-14]. Electrochromic devices based on WO_3 are made of amorphous oxides, while crystalline phase plays a major role in catalysts and sensors [1,15]. Tungsten oxide thin films with nanostructures grains and porosity exhibit high surface area and it accounts for their use as catalysts and sensors [16]. The aim of this work is to synthesis tungsten oxide nanostructures by spin coating technique and study the effect of thin film layers number on the optical and structural properties of prepared films.

2. Materials and methods

To make a solution for spin coating, tungsten powder (99.5% metals basis) and hydrogen peroxide (H_2O_2 , Hydrogen peroxide 30%) was dissolved in de-ionized water bath at 25 °C to avoid agglomeration and more homogenization. After the reaction finished, an evaporative concentration treatment (at 150 °C) was conducted to remove the surplus H_2O_2 . Finally, an appropriate anhydrous ethanol was added into the concentrated solution and the mixed solution was sealed and stirred for 3 h at 70 °C to obtain the WO_3 sgel solution. Before to deposition, the silicon substrate were cleaned using RCA method. In the spin-coating method, substrate which was rotated at

*Corresponding author: asmat_hadithi@uoanbar.edu.iq

300rpm for 60s. The process was repeated for three times to get desired thickness of the film. The annealing process was done at (400 °C).

Surface morphology and structural properties of nanostructures were analyzed using field scanning electron microscopy (FE-SEM), X-ray diffraction (XRD), and energy dispersive X-ray analysis (EDX). Photoluminescence (PL) measurement was also performed at room temperature using an He–Cd laser ($\lambda = 325$ nm),

3. Results and discussion

3.1. X ray diffraction analysis

XRD studies were carried out to get an idea of the nature of the crystal structure of WO_3 thin films on Si substrate prepared by sol-gel technique. Fig (1) and (2) showed the XRD patterns of the annealed and not annealed WO_3 thin films both of (1, 3, and 5) layers. The main crystalline phase, identified by the three main peaks at $2\theta = 14, 28, \text{ and } 44^\circ$ despite of presence of little values of shifting in 2θ value between them due to the difference in the film thickness. These peaks are belonging to hexagonal tungsten oxide (h- WO_3 , JCPDS # 01-075-2187) [17]. The peak situated at 28° can be attributed to the silicon substrate, and also to the contributions of the (111) planes from the hexagonal structures. XRD patterns confirm that adding more layers increased the crystallinity of the material and the annealed films have more intense peaks than those without annealing, that could be attributed to the increase in the crystalline grain size as the small crystals, join each other due to heat treatment also the intensity of XRD peaks related to many factors including the crystallization quality, the density and thickness of thin films[18].

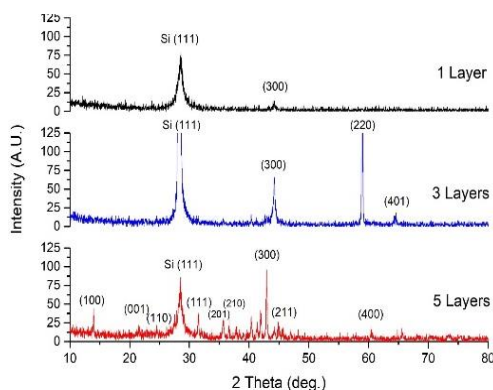


Fig. 1. XRD spectra of the WO_3 thin films deposited on silicon substrate at different layers at 400 °C.

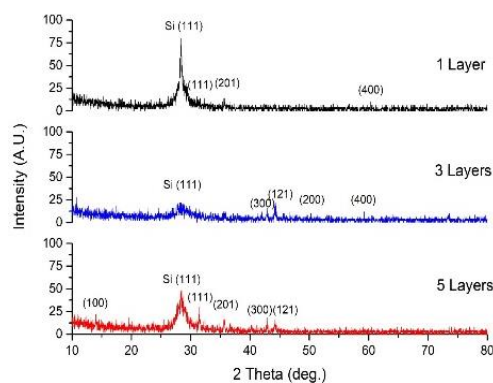


Fig. 2. XRD spectra of the WO_3 thin films deposited on silicon substrate at different layers without annealing.

The lattice constant, and average crystallite size are summarized in Table 1 and 2 for the annealed WO₃ films and not annealed WO₃ films respectively. The average crystallites size was obtained using Scherrer equation (1) based on the highest peak (111),

$$D = \frac{k\lambda}{\beta \cos\theta} \quad (1)$$

where D is the crystal diameter, K = 0.9, $\lambda(\text{Cu K}\alpha) = 1.5405 \text{ \AA}$, θ is the Bragg diffraction angle and β the full width at half maximum (in radians) of the Bragg peaks.

Table 1. XRD pattern analysis of the annealed WO₃ thin films spacing between crystal plans, lattice constant, and average crystallite size.

Layer	2 θ (deg.)	FWHM (deg.)	d _{hkl} (nm)	a (nm)	D (nm)
1	28.37	0.38	0.314	0.543	21.3
3	28.13	0.10	0.316	0.547	81.1
5	28.46	0.64	0.313	0.542	12.7

Table 2. XRD pattern analysis of the not annealed WO₃ thin films spacing between crystal plans, lattice constant, and average crystallite size.

Layer	2 θ (deg.)	FWHM (deg.)	d _{hkl} (nm)	a (nm)	D (nm)
1	28.51	0.82	0.312	0.540	10.2
3	28.16	0.18	0.316	0.547	14.3
5	28.52	0.23	0.312	0.540	35.2

3.2. Atomic Force Microscope (AFM)

Three-dimensional image topography of WO₃ thin films as shown in figure (3,4), which it can be noted from these images a sponge-like structure is produced. The micrographs also show a highly porous structure with conglomerates of grains, which are separated by large irregular voids. The films are made up of spherical grains and that these grains are in good contact with each other if of one-layer thickness then these samples have an increasing in the pore size with increasing of the thickness. In addition, the annealing process has an important effect on the topography structure of WO₃ thin films which can be notes from the increasing of the grains size and that's related to the agglomeration occur due to thermal treatment of the samples.

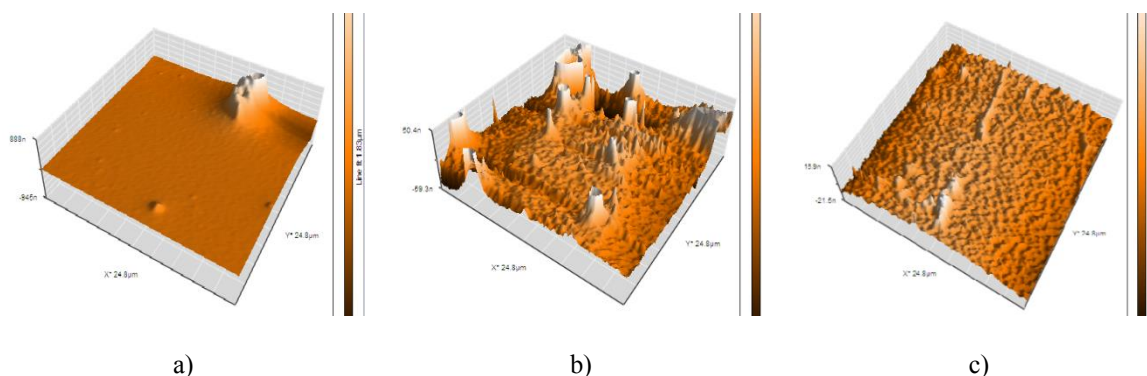


Fig. 3. 3D AFM image for WO₃ with different thickness deposited on silicon substrate without annealing. a) 1 Layer; b) 3 Layers; c) 5 Layer5;

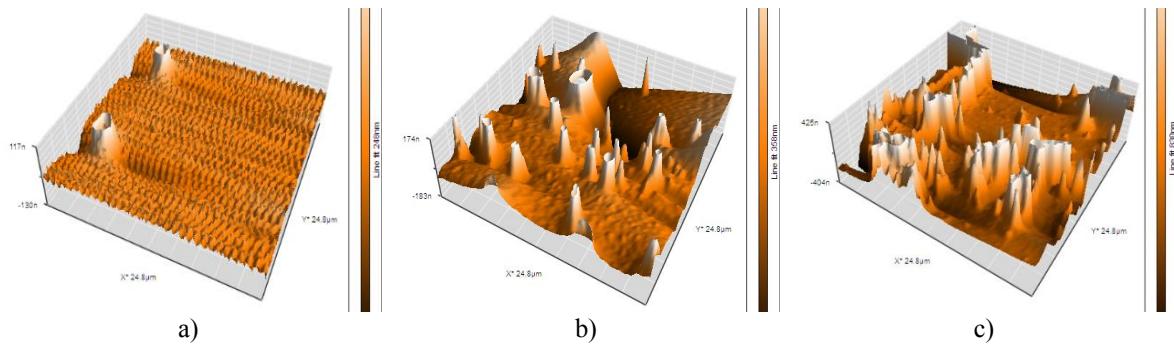


Fig. 4. 3D AFM image and size distributions for WO_3 with different thickness deposited on silicon at $400\text{ }^\circ\text{C}$: a) 1 Layer; b) 3 Layers; c) 5 Layer5;

3.3. Energy Dispersive X-ray Analysis

EDX analysis of the WO_3 films on Si substrates verified the presence of the elements on the films. Strong peaks of W and O indicated that films mainly consisted of WO_3 . The presence of silicon (Si) is caused by the Si substrates, respectively. EDX analysis also indicates that no other element or impurity found in the fabricated sample as shown in Figs. (5, 6 and 7) The elements corresponding to the various peaks are indicated with and without annealing respectively.

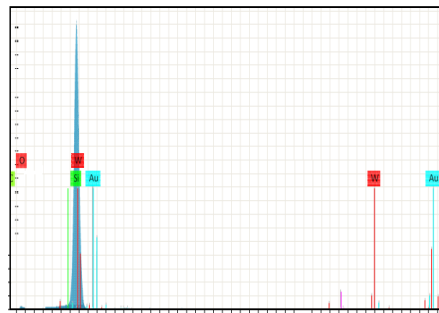


Fig. 5. EDX spectrum of the tungsten coating at 1 Layer.

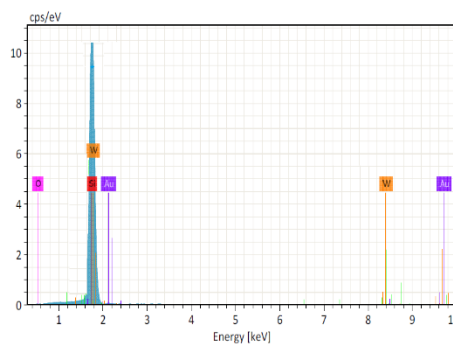


Fig. 6. EDX spectrum of the tungsten coating at 3 Layer.

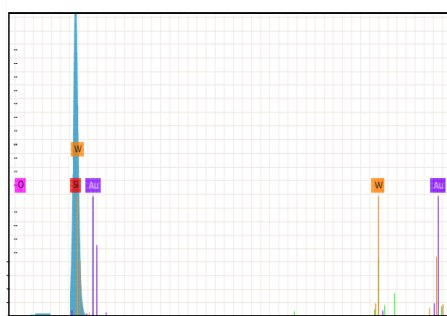


Fig. 7. EDX spectrum of the tungsten coating at 5 Layer.

3.4. Field Scanning Electron Microscopy (FE-SEM)

Fig. 8 illustrated the surface morphology as fine grained structure and unmodified without any cracks and the nanoparticles in the range of nanometers which are visible as bright spots in the images. The films obtained in 1 (a), 3 (b) and 5 (c) layers showed that the WO_3 nanocrystals which are homogeneously dispersed and covering the substrate surface. These films are composed of multifaceted structures that are both large and small. The variation in the thickness does not affect the morphology of the films, but increasing in the number of layers permits a slight increase in the average particle size. These multifaceted crystals are composed of plates that grow radically which present nanometric dimensions with small size distribution.

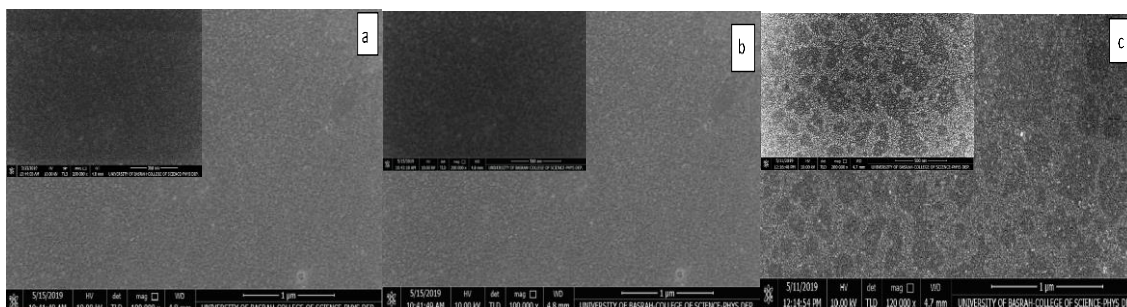


Fig. 8. FE-SEM images of the WO_3/Si thin films deposited at various layers (a) 1 Layer, (b) 3 Layers, (c) 5 Layers at $1\mu m$ and $500 nm$.

3.5. Photoluminescence

Fig. 9 showed the photoluminescence of the WO_3 nanoparticles excited at $300 nm$. It could be observed a broad band located in the visible region, with a maximum wavelength around $356 nm$. It is believed that the particle size, morphology and quantum confinement effect play a role for the room temperature emission. Since the emission properties of WO_3 efficiency increased with numbers of the layer due to absorption was increased with thickness. The results showed the energy gap was increased $3.4-3.48 eV$ and the particle size decrease which due to quantum confinement effect. [19]

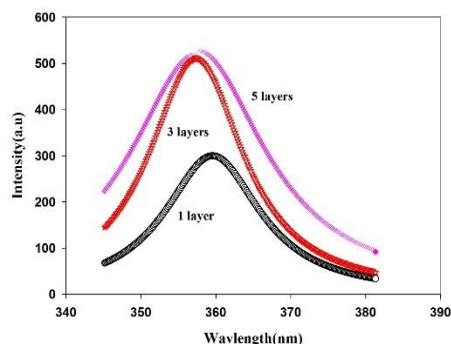


Fig. 9. Photoluminescence spectra WO_3 with different thickness deposited on silicon substrate.

4. Conclusions

The effect of the number of layers and the annealing processing, on morphological and optical properties of WO_3 thin films are studied systematically. XRD patterns consist of characteristic peaks corresponding to hexagonal structures WO_3 phase, suggesting that the crystalline phase in the films has orthorhombic WO_3 . Surface topography studies of the films using AFM determined that the formation of porous, nanostructures thin films, features which make them ideally suitable candidates for gas sensing applications. FE-SEM image showed a homogeneous pattern uniform structures. The analysis of optical properties revealed from in PL measurements showed that the band gap was increased 3.4-3.48 eV. This study was concluded that the structure of WO_3 thin film is effected by the deposition conditions strongly and it is very important to control the of prepared films features.

References

- [1] C. G. Granqvist, Handbook of Inorganic Electrochromic Materials, Elsevier, Amsterdam, 1995.
- [2] A. Ponzoni, E. Comini, M. Ferroni, G. Sberveglieri, Thin Solid Films **8185**, 490 (2005).
- [3] J. S. E. M. Svensson, C. G. Granqvist, Sol. Energy Mater. **11**, 29 (1984).
- [4] A. E. Aliev, H. W. Shin, Solid State Ionics **154–155**, 425 (2002).
- [5] F. A. Cotton, G. Wilkinson, Advanced Organic Chemistry, 5th ed., Wiley, New York, 1988, p. 829.
- [6] B. Stierna, C. G. Granqvist, Appl. Opt. **29**, 117 (1991).
- [7] C. Cantalini, H. T. Sun, M. Faccio, M. Pelino, S. Santucci, L. Lozzi, M. Passacantando, Sens. Actuators B **31**, 81 (1996).
- [8] A. Agarwal, H. Habibi, Thin Solid Films **169**, 257 (1989).
- [9] H. Meixner, J. Gerblinger, U. Lampe, M. Fleischer, Sens. Actuators B **23**, 119 (1995).
- [10] W. Gopel, K. D. Schierbaum, Sens. Actuators B **26–27**, 1 (1995).
- [11] R. Moos, R. Muller, C. Plog, A. Knezevic, H. Leye, E. Irion, T. Braun, K. Marquardt, K. Binder, Sens. Actuators B: Chem. **83**, 181 (2002).
- [12] B. T. Marquis, J. F. Vetelino, Sens. Actuators B **77**, 100 (2001).
- [13] L. Uneus, P. Tobias, P. Salomonsson, I. Lundstrom, A.L. Spetz, Sens. Mater. **11**, 305 (1999).
- [14] Y. K. Chung, M. H. Kim, W. S. Um, H. S. Lee, J. K. Song, S. C. Choi, K. M. Yi, M. J. Lee, K. W. G. Chung, Sens. Actuators B: Chem. **60**, 49 (1999).
- [15] M. D. Antonik, J. E. Schneider, E. L. Wittman, K. Snow, J. F. Vetelino, R. J. Lad, Thin Solid Films **256**, 247 (1995).
- [16] O. Alm, L. Landstrom, M. Boman, C. G. Granqvist, P. Heszler, Appl. Surf. Sci. **247**, 262 (2005).
- [17] Irene T.S. Garcia, Diogo S. Corrêa, Diego S. de Moura, Julia C. O. Pazinato, Marcelo B. Pereira, Nadja B. D. da Costa, Journal of the Brazilian Chemical Society **25**(5),

- 822 (2014).
- [18] I. T. Garcia, D. S. Corrêa, D. S. de Moura, J. C. Pazinato, M. B. Pereira, N. B. da Costa, *Surface and Coatings Technology* **283**, 177 (2015).
- [19] Asmiet Ramizy, Z. Hassana, Khalid Omar, Y. Al-Douri, M. A. Mahdi, *Applied Surface Science* **257**, 6112 (2011).